The alteration of intra-ligand donor-acceptor interactions through torsional connectivity in substituted Re-dppz complexes

Bethany Adams[2], Georgina E. Shillito[1], Holly van der Salm[1], Raphael Horvath[2], Christopher B. Larsen[1], Nigel T. Lucas[*1], Michael W. George[*2], Keith C. Gordon[*1].

[1]Department of Chemistry, University of Otago, P.O. Box 56, Dunedin, New Zealand

[2]School of Chemistry, University of Nottingham, University Park, Nottingham, NG7 2RD, U.K.

ABSTRACT: The ground and excited properties of a series of $[ReCl(CO)_3(dppz)]$ complexes with substituted donor groups have been investigated. Alteration of donor-acceptor communication through modulation of torsional angle and the number and nature of the donor substituent allowed the effects on the photophysical properties to be characterized though both computational and spectroscopic techniques, including TD-DFT, resonance Raman and time resolved infrared. The ground state optical properties show significant variation as a result of donor group modulation, with increased angle between the donor and acceptor blue-shifting and depleting the intensity of the lowest energy transition, which was consistently ILCT in nature. However, across all complexes studied there was minimal perturbation to the excited state properties and dynamics. Three excited states on the picosecond, nanosecond and microsecond time scales were observed in all cases, corresponding to ^{1}ILCT, ππ* and ^{3}ILCT respectively.

Introduction.

There is a large amount of activity in fundamental and applied research in trying to ultilise solar photons to drive chemistry, which ultimately relies on understanding and controlling molecular excited states. Transition metal diimine complexes such as $[Ru(bpy)_3]^{2+}$ have been widely exploited because of their long-lived ^{3}MLCT excited states and this has led to many applications including the recent resurgence in photo-redox catalysis.[1] The incorporation of organic and inorganic components to synthesise metal–organic chromophores without forming a metal–carbon bonds is a promising approach to producing new photofunctional molecules.[2-3] The outstanding properties of metal-dppz (dppz = dipyrido[3,2-a:2′,3′-c]phenazine)) complexes have been exploited to produce long-lived charge separated excited states. Dppz (Figure 1) has been a previously studied system because of the nature of its electronic structure in which the unoccupied MOs show a level of segregation over differing sections of the ring system.

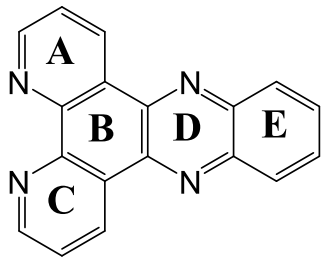

Figure 1. Structure of dipyrido[3,2-a:2′,3′-c]Phenazine (dppz).

One of the MOs is based on the phenazine (phz) rings (B, D and E) and the other on the phenanthroline (phen) rings (A, B, and C). In metal complexes the low energy absorption properties are dominated by the M → dppz(phen) MLCT transition as there is no overlap between the metal d orbitals and the dppz(phz) MO.[4-5] However the dppz(phz) MO is occupied after photoexcitation.[6-10] This electronic structure leads to a number of interesting properties, for example both ruthenium(II)[5, 11-12], platinum(II)[13] and rhenium(I)[8] complexes show differing photophysics on going from a protic solvent to an aqueous solvent with DNA present, with the MLCT(phz) being a dark state and the MLCT(phen) a bright, emissive, state.[11, 14] In the later mixture, strong emission is observed as the dppz intercalates into the DNA.[15] This is due to the interplay between the lowest lying excited states in these compounds. These can be MLCT(phz), MLCT(phen) or ligand-centered in nature.[11, 14] For $[Ru(bpy)_2(dppz)]^{2+}$ it has been shown that the MLCT(phz) is enthalpically favoured and the MLCT(phen) entropically. In dppz the unoccupied MOs lie close in energy but they can be tuned by suitable substitution, commonly at the 10, 11, 12, 13 positions (ring E to tune the phz MO) or at the 3,6 or 2,7 positions on ring A to tune the phen MO. A number of studies have investigated the effects of placing electron withdrawing groups at these positions.[16]

The effect of coupling strong electron donor groups to the dppz framework has been previously investigated and studies on thiofulvalene moieties fused to the E-ring show that a there are strong intraligand charge-transfer (ILCT)

transitions with these types of groups.[17-20] Carbazole electron donating groups have been used at 10, 13 positions to also create strong ILCT bands that involve the donor group and the dppz(phz) MO.[21] Pt complexes with these ligands show deep red emission and such ligands themselves showed a wide range of emission wavelengths based on the type of substituent used. In a comprehensive study of dppz with TPA group or TPA-thiophene group substitution at the 3, 6 and/or 10, 13 positions Wang et al[22] showed that the optical transitions could be tuned by 1 eV and the Stokes shift ($\tilde{\nu}$abs – $\tilde{\nu}$em) from 3500 to 10500 cm^{-1}. The use of π-conjugated donor groups has changed the range of energies for the dppz MOs but also introduced new MOs that affect in a direct way the electronic structure. These types of donor-acceptor systems provide opportunities to manipulate properties because of the nature of the acceptor MOs on the dppz ligand. Raman, time-resolved Raman and IR spectroscopic techniques are very powerful techniques for use in unravelling the complex photophysics of metal-dppz complexes.[23] We used such approaches to investigate how the photophysics of substitution of dppz by TPA in the 11-position resulted in both the ligand and Re(CO)3Cl complex having near identical absorbing and emitting states.[24] These were both ^{3}ILCT in nature i.e. TPA → dppz(phz) charge-transfer. This finding was supported by the resonance Raman spectra which showed identical resonance enhancement patterns form ligand to complex meaning that the absorbing state was dominated by an ILCT chromophore, the emitting states showed solvatochromic behaviour with similar Stokes shifts as a function of solvent. Time-resolved infrared spectra showed the shift in ν(CO) bands of the complex on going from the ground to the excited state was consistent with a ligand-centred excited states and two close lying states with the same electronic nature were identified. Substituting the TPA with CN and OMe substituents at the phenyl para positions of the TPA it was possible to tune the emission across the entire visible spectrum by using the substituents and solvent.[25] However in all cases the dominant absorbing and emitting states were ILCT in nature. It is also possible to alter the interaction between the dppz and TPA via differing linking groups. This has been done for $[Ru(bpy)_2(dppz\text{-}linker\text{-}TPA)]^{2+}$ complexes.[26] In this study the resonance Raman spectra at wavelengths towards the blue edge of the lowest energy absorption band, show enhancements of bpy and dppz-linker-TPA modes as the Ru → bpy MLCT transitions are intense and complicate the absorbing chromophores present. TD-DFT calculations on these systems reveal that the lowest energy transition is TPA → dppz(phz) irrespective of the linker of the complexation to the metal. Furthermore the lowest excited state is shown to be the same for dppz-TPA, $[ReCl(CO)_3(dppz\text{-}TPA)]$ and $[Ru(bpy)_2(dppz\text{-}TPA)]^{2+}$ as the excited state resonance Raman spectra of all three of these materials are identical with distinct bands that may be attributed to $TPA^{\cdot+}$.[26]

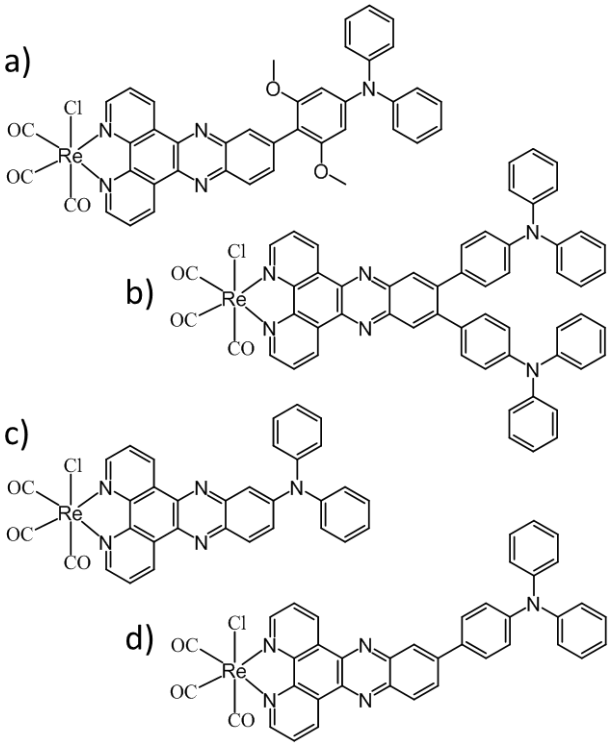

Figure 2. Complexes investigated in this study; a) $[ReCl(CO)_3(dppz\text{-}(OMe)_2TPA)]$, b) $[ReCl(CO)_3(dppz\text{-}(TPA)_2)]$, c) $[ReCl(CO)_3(dppz\text{-}NPh_2)]$, d) $[ReCl(CO)_3(dppz\text{-}TPA)]$.

In this study we have compared the interaction between NPh_2 and TPA donors and dppz in a systematic fashion by altering the steric interactions between the units.

Electronic Absorption Spectroscopy and TD-DFT. The electronic absorption spectra of the ligands and their respective complexes in CH_2Cl_2 are presented in Figure 3. Complexation to the $ReCl(CO)_3$ centre results in a red-shift in the absorption band but does not cause any significant changes to the shape of the spectral profile. The absorbing and emitting states for all compounds studied show significant solvatochromic behavior with large Stokes shifts, suggestive of a significant change in dipole, $\Delta\mu$ associated with the transition. This was explored further via conduction of a Lippert-Mataga analysis with the $\Delta\mu$ values obtained presented in Table 1. The $\Delta\mu$ values for the ligands and their respective complexes are similar. This is suggestive that the predominant charge transfer character is ligand based, with complexation to the metal centre resulting in minimal change. The $\Delta\mu$ for the dppz-NPh_2 ligand and its complex are significantly less than that of the other compounds. This is attributed to lack of a complete TPA donor group and hence while the transition is still ILCT based, the separation of the electron distribution across the compound is less distinct, as shown in Figure 4 and hence there is less CT contribution to the transition compared to the other compounds possessing full TPA donor groups.

Table 1. Experimental and TD-DFT (CAM-B3LYP/6-31g(d)) calculated data for the ligands and complexes in CH_2Cl_2.

	Experimental			Calculated				
	λ / nm	ε / 10^3 M^{-1} cm^{-1}	Δμ / D	λ / nm	*f*	MO contribution	D-A angle	Δμ / D
dppz-NPh2	476	18.8	10 ± 2	343	0.438	H→L (89%)	27.5 °	7
dppz-TPA	457	16.9	22 ± 2	316	0.718	H→L (77%)	30.2 °	3
dppz-(OMe2)TPA	434	11.6	20 ± 4	326	0.576	H→L (69%), H-2→L(19%)	40.3 °	5
dppz-(TPA)2	457	18.1	22 ± 4	315	0.675	H→L (77%), H-3→L(16%)	46.3 °	31
[ReCl(CO)3(dppz-NPh2)]	499	26.2	13 ± 2	412	0.562	H→L (87%)	22.8°	12
[ReCl(CO)3(dppz-(TPA)]	488	18.2	25 ± 1	390	0.780	H→L (75%), H-3→L (13%)	34.4°	26
[ReCl(CO)3(dppz-(OMe)2TPA)]	469	10.6	22 ± 8	386	0.586	H→L (70%), H-4→L (15%)	51.9°	21
[ReCl(CO)3(dppz-(TPA)2)]	493	20.0	25 ± 4	398	0.868	H→L (76%), H-4→L (10%)	49.6°	30

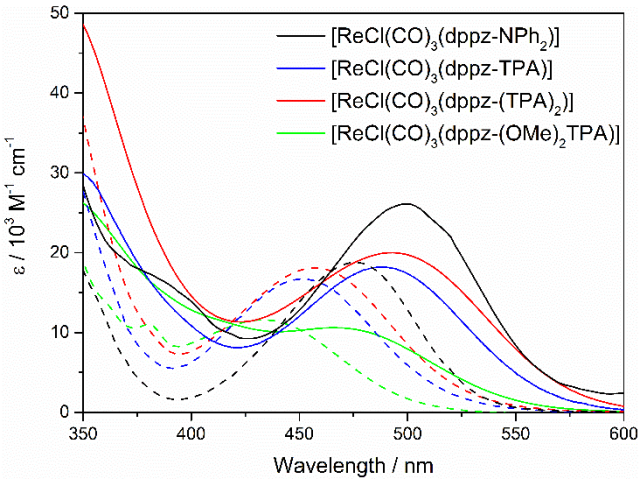

Figure 3. Electronic absorption spectra, measured in CH_2Cl_2 of the ligands (dashed) and complexes (solid) studied.

$[ReCl(CO)_3(dppz\text{-}NPh_2)]$ displays both the greatest red-shift and highest oscillator strength for the lowest energy transition, followed by that of $[ReCl(CO)_3(dppz\text{-}(TPA)]$ and $[ReCl(CO)_3(dppz\text{-}(TPA)_2)]$. The addition of sterically bulky OMe groups to the TPA unit alters the angle between the TPA donor and the dppz acceptor from 34.4 to 51.9 i.e. by 17.5°, disrupting the D-A conjugation, thereby increasing the transition energy. This drop in oscillator strength is likely also attributed to the increase in D-A angle as a result of poorer overlap of the frontier molecular orbitals involved in the lowest energy transition. This is supported by TD-DFT calculations (Table 1), which replicate the observed trend in the relative absorption energies. The addition of a second TPA donor group, causes a slight red shift and increase in oscillator strength for the lowest energy transition. Although the addition of a secondary TPA group causes an increase in the D-A torsional angles for $[ReCl(CO)_3(dppz\text{-}(TPA)_2)]$, the complex exhibits an absorption that is slightly red-shifted and increased in intensity relative to that of the single donor complex, $[ReCl(CO)_3(dppz\text{-}(TPA)]$. It is suggested that the disruption in D-A conjugation caused by the increased D-A angle is compensated for by the addition of a secondary donor group. The TD-DFT calculations predict that the lowest energy state is consistently ILCT in nature, with the HOMO is predicted to lie on the TPA/NPh_2 donor substituent and the LUMO is predominantly dppz(phz) based. However, the calculations also indicate that the lowest energy transition is not entirely H→L in nature. The differences in the relative contribution of configuration interactions to the transition are manifested in the electronic absorption spectra, with an increasing contribution from the more delocalized H-3 or H-4 MOs to the transition, coinciding with an increase in transition energy. Likewise, the involvement of the H-3 and H-4 MOs suggest a minor contribution from the $ReCl(CO)_3$ centre, which can be observed through slight enhancement of the CO based vibrational modes at blue excitation wavelengths in the complexes' resonance Raman spectra.

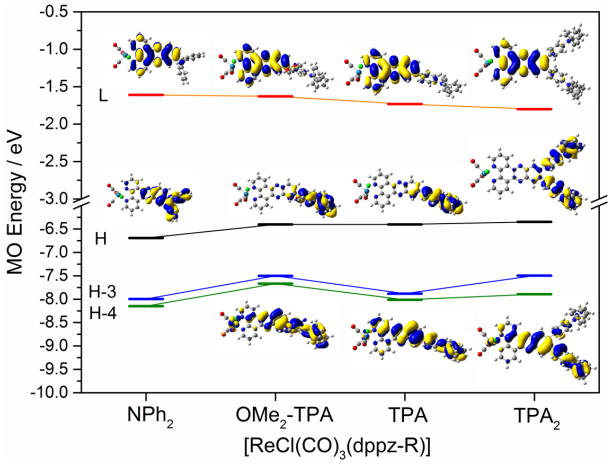

Figure 4. TD-DFT calculated (CAM-B3LYP, 6-31g(d), in a CH_2Cl_2 solvent field) frontier molecular orbitals of the complexes studied.

Resonance Raman Spectroscopy. The electronic nature of the Franck-Condon state can be probed using resonance Raman spectroscopy. Raman spectra of the ligands and respective complexes where measured at various excitation wavelengths across the lowest energy absorption band. The relative enhancement of characteristic vibrational modes compared to that on the non-resonant spectrum taken at 1064 nm, provide an indication of the nature of the electronic transition occurring in that region.[27-28] The resonance Raman spectra of $[ReCl(CO)_3(dppz\text{-}TPA)]$ has been reported previously[24] and showed little spectral variation across the lowest en-

ergy absorption band, with the spectra dominated by TPA modes and dppz(phz) modes, indicating that the Franck-Condon state was dominated by a single ILCT transition from the TPA donor to the dppz acceptor, with very minimal indication of metal involvement in the blue region of the absorption band. The resonance Raman spectra of [ReCl(CO)$_3$(dppz-(OMe)$_2$TPA)] are presented in Figure 5.

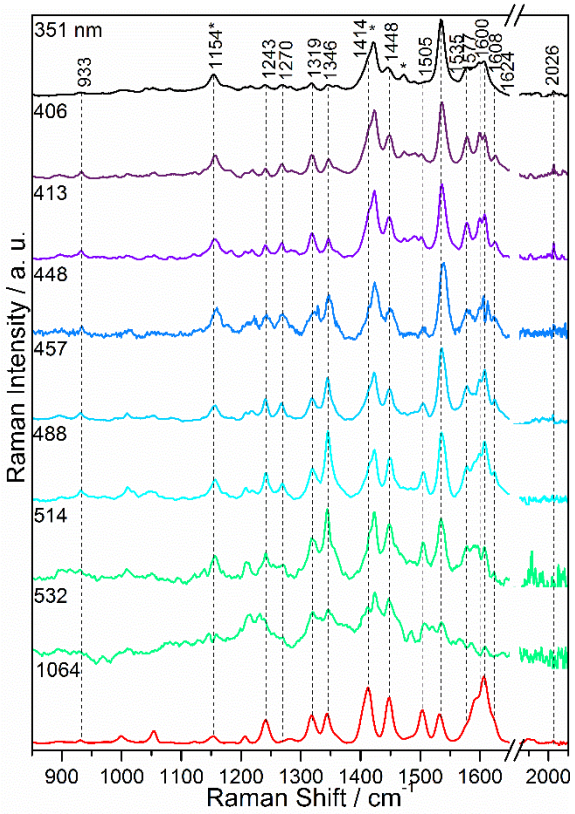

Figure 5. Resonance Raman spectra of [ReCl(CO)$_3$(dppz-(OMe)$_2$TPA)] at various excitation wavelengths. CH_2Cl_2 solvent bands marked with *.

Between 351 and 457 nm excitation, the spectra are dominated by the 1535 cm^{-1} dppz(phz) based mode and there is a slight enhancement of the totally symmetric carbonyl stretching mode at 2026 cm^{-1} which is visible up to 457 nm. In contrast, the bands at 1270, 1600 and 1608 cm^{-1}, predominantly associated with vibration of the TPA moiety are diminished in intensity relative to that of the non-resonant spectrum. This suggests a lack of involvement of the TPA unit in this region, with the transition likely being ππ* in nature, shown by enhancement of dppz based modes, with a minor MLCT contribution indicated by slight enhancement of the 2026 cm^{-1} CO band. As the λ_{ex} increases to 488 nm, the enhancement pattern changes, with the 1270, 1600 and 1608 cm^{-1} TPA modes increasing in intensity as well as more delocalized dppz-TPA vibrations at 1243 and 1346 cm^{-1} and dppz(phz) modes at 1448 and 1624 cm^{-1}. The 1535 cm^{-1} dppz(phz) band also maintains intensity in this region. The 1154 cm^{-1} band is also enhanced and is likely associated with vibration of the TPA unit however it is also coincident with a CH_2Cl_2 solvent band. The bands decrease in intensity as λ_{ex} extends to the tail end of the electronic absorption band. The pattern of relative enhancement of both TPA and dppz(phz) modes is consistent with the presence of a dominant ILCT state across the lowest energy absorption band, with the higher energy tail end likely composed of a ππ* state, with a minor MLCT contribution, which is consistent with that predicted by TD-DFT.

The resonance Raman spectra of [ReCl(CO)$_3$(dppz-(TPA)$_2$)] shows similar features (see ESI) to that of [ReCl(CO)$_3$(dppz-(OMe)$_2$TPA)], with the lowest energy transition being ILCT in nature, with a higher energy MLCT also present. The bands at 1601 and 1608 cm^{-1} in the resonance Raman spectra of [ReCl(CO)$_3$(dppz-NPh$_2$)] (see ESI) were weaker compared to the other complexes, likely due to lack of a complete TPA group, with the vibrations involving only the two nitrogen coordinated phenyl groups. The 2035 cm^{-1} CO band is no longer visible at λ_{ex} > 406 nm. Comparison between the resonance Raman spectra of [ReCl(CO)$_3$(dppz-(OMe)$_2$TPA)] and the previously reported [ReCl(CO)$_3$(dppz-TPA)],[29] suggests that as the D-A angle is increased, there is an increased MLCT contribution to the transition, indicated by enhancement of CO vibrations at longer excitation wavelengths. Furthermore, the ILCT state is increased in energy, with TPA mode enhancement occurring at shorter wavelengths. This is consistent with both the electronic absorption spectra and TD-DFT calculations. Nonetheless, the dominant, lowest energy transition in all complexes is ILCT in nature.

Transient Absorption Spectroscopy. Transient absorption maps of the [ReCl(CO)$_3$(dppz-R)] complexes recorded are presented in Figure 6. The TA maps are recorded 250 ns after initial excitation and other than a reduction in intensity, show no significant change to their spectral shape over time. The kinetic traces show monoexponential decay to the ground state, with excited state lifetimes on the microsecond timescale observed. These data suggest that a single, long-lived state is being measured.

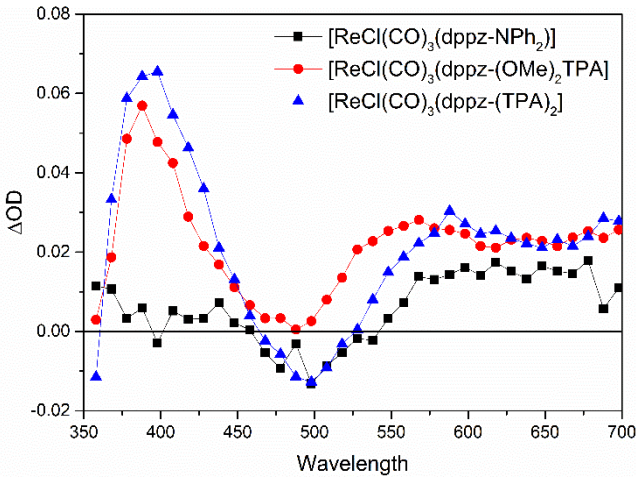

Figure 6. Transient absorption maps of the complexes studied using 355 nm excitation. Spectra were taken 250 ns after excitation and recorded in CH_2Cl_2.

The TA maps display spectral features different to those of Re(I) complexes without an electron donating substit-

uent coordinated to the dppz ligand.[30] The primary difference being the presence of a positive transient signal between *ca.* 550-700 nm observed in the studied complexes which is not present in the unsubstituted species, thereby indicating involvement of the electron donating moiety to the long lived excited state measured. This is most clearly observed for $[ReCl(CO)_3(dppz\text{-}(OMe)_2TPA)]$ and $[ReCl(CO)_3(dppz\text{-}(TPA)_2)]$ which display a prominent positive transient signal at λ_s > *ca.* 500 nm and 525 nm respectively, similar to that observed in the previously reported compounds containing a TPA substituted dppz moiety and has been attributed to the presence of $TPA^{\bullet+}$.[24, 26] As discussed previously, $[ReCl(CO)_3(dppz\text{-}NPh_2)]$ lacks a full TPA donor group, however it still displays positive features towards the red, suggesting likely involvement of the NPh_2 substituent to the transition. The excited state probed in the TA measurements is assigned as a long lived ^{3}ILCT state for all complexes. The presence of other, shorter lived states were unable to be detected through TA measurements due to convolution with the laser pulse. However the presence of other, shorter lived species was able to be detected and characterized through the use of TRIR spectroscopy.

Time-resolved Infrared Spectroscopy. The photophysical properties of $[ReCl(CO)_3(dppz\text{-}NPh_2)]$, $[ReCl(CO)_3(dppz\text{-}(OMe)_2TPA)]$ and $[ReCl(CO)_3(dppz\text{-}(TPA)_2)]$ were probed on the picosecond and nanosecond time scales using time-resolved infrared spectroscopy (TR-IR). Across all the complexes, the TRIR data revealed the presence of three electronic excited states, which possess excited state lifetimes on the picosecond, nanosecond and microsecond timescales respectively. The lifetime of the latter state is consistent with the TA measurements above and is assigned to ^{3}ILCT.

The TRIR spectra of $[ReCl(CO)_3(dppz\text{-}NPh_2)]$ obtained after 355 nm photoexcitation at several time delays are presented in **Figure 7.**

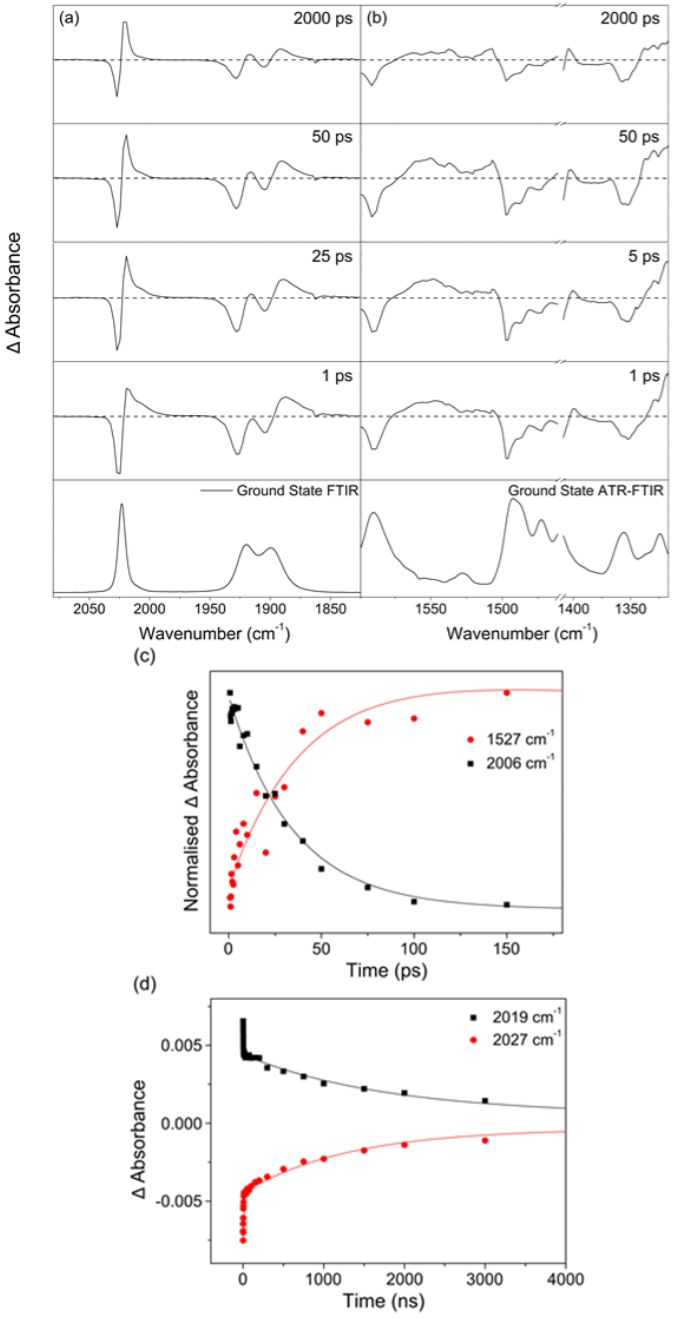

Figure 7. TRIR spectra of $[Re(CO)_3Cl(dppzNPh_2)]$ acquired in CH_2Cl_2 in in the ν(CO) stretching region (a) and in the fingerprint region (b). Kinetics of relevant bands are shown on the picosecond timescale (c) and nanosecond timescale (d).

The TRIR spectra obtained 1 ps after photoexcitation clearly show that the parent bands are bleached (2027, 1925, 1899 cm^{-1}) and transient peaks are formed at 2016, 2006 and 1888 cm^{-1}, which subsequently shift to slightly higher energies. There is a prominent shoulder at *ca.* 2006 cm^{-1} which decays at the same time {τ = 37 (± 2) ps} as a band is formed at 2019 cm^{-1} {τ = 40 (± 2) ps}. The lower energy parent bleach appears to recover. However, we assign this be due to overlap of the parent and new transient features since the amount of recovery/growth varies

Table 2. Summary of the exited state TRIR bands observed after photoexcitation at 355 nm.

$\nu_{(CO)}$ / cm^{-1}	$\nu_{(ligand)}$ / cm^{-1}	$\tau_{(growth)}$ / ns	$\tau_{(decay)}$ / ns	Assignment
$[ReCl(CO)_3(dppz\text{-}NPh_2)]$				
2006	1590[a], 1575[a], 1488[a], 1397[a]		0.037 (± 0.002)	^{1}ILCT
2019, 1888	1560, 1549, 1504[a], 1403[a]		2.5 (± 0.3)	ππ*
2020, 1891	1563[a], 1537, 1507, 1404	0.04 (± 0.002)	1500 (± 300)	^{3}ILCT
2024, 1920, 1899	1589, 1527, 1492, 1473, 1356, 1325			Ground State (FTIR)
$[ReCl(CO)_3(dppz\text{-}(OMe)_2TPA)]$				
2006			0.043 (± 0.006)	^{1}ILCT
2018, 1887	1554, 1311		2 (± 1)	ππ*
2019, 1890	1542, 1505, 1470	0.027 (± 0.005)	2900 (± 500)	^{3}ILCT
2024, 1922, 1899	1584, 1568, 1488, 1413, 1353, 1342	-	-	Ground State (FTIR)
$[ReCl(CO)_3(dppz\text{-}(TPA)_2)]$				
2005			0.028 (± 0.004)	^{1}ILCT
2019, 1886	1583[a], 1563, 1551[a]		1.5 (± 0.5)	ππ*
2019, 1887	1570, 1537, 1504, 1489, 1479, 1341[a]	0.03 (± 0.01)	2200 (± 600)	^{3}ILCT
2027, 1928, 1903	1587, 1509, 1486, 1356, 1319	-	-	Ground State (FTIR)

[a]Identified from global analysis.

across the parent bleach. More detailed analysis and band fitting suggest that a band decays at 1888 cm^{-1} to form a band at 1891 cm^{-1} with an additional decay and growth occurring around 1920 cm^{-1}. The initial transient with a band at 2006 cm^{-1} and the secondary product characterised by an absorption at 2019 cm^{-1} are assigned to different states and this is further confirmed using global analysis (see ESI). The behaviour and inter-conversion between these two states is similar to that of a recent report on rhenium complexes based on a number of 3-R-1-(2-pyridyle)-imidazol[1,5-α]pyridine (dmpy) ligands by Blanco-Rodrgiuez *et al*[31], wherein two new vibrational bands were found at lower energy with respect to the parent. They observed that on the timescale of tens of picoseconds there was conversion of two states, where the lowest energy ν(CO) band decreased in intensity as the higher energy band drew in and this process was attributed to an unusually slow ISC from S_1 to T_1 of ligand centred states of a metal complex. This unusual observation of slow ISC of a metal based Re-diimine excited states was explained by symmetry constraints on the spin-orbit coupling, whereby the Re metal was thought of as isolated from the ligand moiety.

The TRIR data, in conjunction with the resonance Raman, Lippert-Mataga and transient absorption data suggests assignment of the picosecond and microsecond states as ^{1}ILCT and ^{3}ILCT respectively, where there is little interaction with the metal centre in these states. The precise nature of the ligand based excited states is difficult to glean from the ν(CO) bands alone. This has been explored further by correlating these results with measurements in the IR fingerprint region. On the nanosecond timescale, the TRIR bands at 2019 and 1888 cm^{-1} exhibit a bi-exponential decay {τ = 2.2 (± 0.2) ns and 1800 (± 100) ns}, as shown in Figure 4. The lifetimes are in good agreement with the parent recovery {2.3 (± 0.5) ns and 2200 (± 500) ns} where the latter corresponds to ^{3}ILCT decaying back to the ground state. We tentatively assign the nanosecond transient to a ππ* state but the dynamic interplay between these states is unclear. From the ν(CO) TRIR kinetics alone it is difficult to unambiguously assign, however unlikely, whether: (i) ^{1}ILCT decays to the ^{3}ILCT and ππ* excited states; (ii) ^{1}ILCT decays to the ππ* excited state which subsequently decays to ^{3}ILCT excited state; or (iii) ^{1}ILCT and ππ* are formed simultaneously and ^{1}ILCT decays to ^{3}ILCT. The spectral shifts in the ν(CO) bands to lower energies exhibited by all observed states are indicative of an increase in electron density in the carbonyl antibonding orbitals. This is consistent with presence of both dppz-centred ππ* and ILCT states.[30, 32-33] The data in the fingerprint region should inform on both the natures of the ligand-based excited states and their kinetics.

Table 2. At early times there are many subtle changes but there are clear bands at 1537, 1507, and 1404 cm^{-1}, which are formed at similar times {40 (± 10) ps} as the shoulder at 2006 cm^{-1} decays {37 (± 2) ps} and these are marker bands for formation of ^{3}ILCT state. There is also evidence for two overlapping bands around the 1550 cm^{-1} region,

In the fingerprint region a number of bleaches corresponding to the ground state spectra are observed after photoexcitation at 355 nm (**Figure** 7), together with a number of excited state features, which are summarised in

consistent with the decay of the ^{1}ILCT state to the ^{3}ILCT state. The bands at 1537, 1507, and 1404 cm^{-1} decay on the microsecond timescale as the parent bands fully reform {2.3 (± 0.5) μs}. There is a distinct band at ca. 1549 cm^{-1} which decays on the nanosecond timescale {2.2 (± 0.2) ns}.

The photophysics of $[Re(CO)_3Cl(dppzNPh_2)]$ have been investigated further by performing global analyses on the TRIR data and the results are shown in the ESI. The global analyses show the presence of three states, with lifetimes of 30 ps, 2.2 ns and 1400 ns which is consistent with the single point kinetics described above. Furthermore, the initial state possesses peaks at 2009 and 1879 cm^{-1}, which are consistent with the observed features at 2006 and 1880 cm^{-1} at early times and are assigned above to ^{1}ILCT. The global analysis predicts additional states to possess very similar IR spectra to those observed for the ^{3}ILCT and ππ* states, with excited state bands at 2018, 1916 and 1892 cm^{-1}. It is also evident from these data that ^{3}ILCT and ππ* are indistinguishable by analysis of the ν(CO) region. However, significant differences exist in the fingerprint region. The initial process is predicted to show Table **2**. Similar excited state behaviours to that of $[Re(CO)_3Cl(dppz\text{-}NPh_2)]$ are observed, with both complexes showing three distinct states, to which analogous assignments can be made. Marker bands for ππ* are observed at 1554 and 1551 cm^{-1} for $[ReCl(CO)_3(dppz\text{-}(OMe)_2TPA)]$and $[ReCl(CO)_3(dppz\text{-}(TPA)_2)]$ respectively, however, for the latter an even stronger additional band at 1563 cm^{-1} is present. As this complex possesses two TPA donor units it is reasonable to assume that changes in bonding on this part of the complex differs significantly compared to the complexes containing only a single TPA donor or a NPh_2 group. Finally, the ^{3}ILCT state shows additional unique bands for $[ReCl(CO)_3(dppz\text{-}(OMe)_2TPA)]$and $[ReCl(CO)_3(dppz\text{-}(TPA)_2)]$ at 1470 and 1570 cm^{-1} respectively, indicating the differences in bonding that exist for these complexes. Common bands for ^{3}ILCT for all three complexes exist at ca. 1540 and 1505 cm^{-1}.

decay of bands at 1575, 1488 and 1397 cm^{-1}, with simultaneous growth of features at 1559, 1549, 1534, 1506, and 1404 cm^{-1}, assigned to the conversion of ^{1}ILCT to ^{3}ILCT. For ππ* the above-mentioned band at 1549 cm^{-1} as well as bands at 1560, 1504 and 1403 cm^{-1} are present, while ^{3}ILCT is most prominently characterised by bands at 1537 and 1507 cm^{-1}. In summary we interpret our results to show that we initially form ^{1}ILCT and ππ*, where ^{1}ILCT decays to ^{3}ILCT and states ^{3}ILCT and ππ* independently decay back to the ground state.

The TRIR spectra of $[ReCl(CO)_3(dppz\text{-}(OMe)_2TPA)]$ and $[ReCl(CO)_3(dppz\text{-}(TPA)_2)]$ are presented in ESI, with the respective band positions and lifetimes summarised in

Conclusion.

We have shown that for a range of dppz complexes with differing donor groups there are distinct changes in the optical properties of the ground state. Substitution of methoxy groups to the TPA substituent increase torsional angle between the donor and acceptor, resulting in a decrease in the extinction coefficient for the lowest energy transition and a blue shift in that absorption. However for each of these complexes there are common excited state properties with three distinct states namely a ^{1}ILCT, ^{3}ILCT and ππ* observed on the picosecond, microsecond and nanosecond timescales respectively. Photoexcitation populates the ^{1}ILCT and ππ* states. The ^{1}ILCT interconverts to the ^{3}ILCT state. The ππ*state is independent of the ILCT states. Changing the nature of the donor group from NPh_2 to substituted TPA produces qualitatively similar results both in terms of the nature of the excited states and their subsequent dynamics but the limited range of compounds studied means that it is difficult to generate generic conclusions on such trends and further studies are ongoing to elucidate fully the effects of the nature and number of donor groups together with the coupling (torsional angle and distance) on the dynamics of these long-lived charge separated states.

ASSOCIATED CONTENT

Supporting Information. Resonance Raman spectra, TRIR spectra, experimental de-tails, X-ray crystallography, synthetic scheme. This material is available free of charge via the Internet at http://pubs.acs.org.

AUTHOR INFORMATION

Corresponding Author

Prof Keith C. Gordon
Email: keith.gordon@otago.ac.nz
Prof Michael W. George
Email: mike.george@nottingham.ac.uk
Dr Nigel T. Lucas
Email: nlucas@chemistry.otago.ac.nz

Author Contributions

The manuscript was written through contributions of all authors. / All authors have given approval to the final version

of the manuscript. / ‡These authors contributed equally. (match statement to author names with a symbol)

Funding Sources

Support from the University of Otago and the MacDiarmid Institute for Advanced Materials and Nanotechnology

Notes

Any additional relevant notes should be placed here.

ACKNOWLEDGMENT

(Word Style "TD_Acknowledgments"). Generally the last paragraph of the paper is the place to acknowledge people (dedications), places, and financing (you may state grant numbers and sponsors here). Follow the journal's guidelines on what to include in the Acknowledgement section.

ABBREVIATIONS

CCR2, CC chemokine receptor 2; CCL2, CC chemokine ligand 2; CCR5, CC chemokine receptor 5; TLC, thin layer chromatography.

REFERENCES

(Word Style "TF_References_Section"). References are placed at the end of the manuscript. Authors are responsible for the accuracy and completeness of all references. Examples of the recommended formats for the various reference types can be found at http://pubs.acs.org/page/4authors/index.html.

---

1. Stephenson, C.; Yoon, T. *Acc. Chem. Res.* **2016,** *49*, 2059-2060.
2. Schanze, K. S.; Walters, K. A. *Mol. Supramol. Photochem.* **1998,** *2*, 75-128.
3. Castellano, F. N. *Acc. Chem. Res.* **2015,** *48*, 828-839.
4. Amouyal, E.; Homsi, A.; Chambron, J.-C.; Sauvage, J.-P. *J. Chem. Soc., Dalton Trans.* **1990,** 1841-1845.
5. Friedman, A. E.; Chambron, J. C.; Sauvage, J. P.; Turro, N. J.; Barton, J. K. *J. Am. Chem. Soc.* **1990,** *112*, 4960-4962.
6. van der Salm, H.; Fraser, M. G.; Horvath, R.; Cameron, S. A.; Barnsley, J. E.; Sun, X. Z.; George, M. W.; Gordon, K. C. *Inorg. Chem.* **2014,** *53*, 3126-40.
7. van der Salm, H.; Larsen, C. B.; McLay, J. R.; Fraser, M. G.; Lucas, N. T.; Gordon, K. C. *Dalton Trans* **2014,** *43*, 17775-85.
8. Cao, Q.; Creely, C. M.; Davies, E. S.; Dyer, J.; Easun, T. L.; Grills, D. C.; McGovern, D. A.; McMaster, J.; Pitchford, J.; Smith, J. A.; Sun, X.-Z.; Kelly, J. M.; George, M. W. *Photochem. Photobiol. Sci.* **2011,** *10*, 1355-1364.
9. Kuimova, M. K.; Alsindi, W. Z.; Blake, A. J.; Davies, E. S.; Lampus, D. J.; Matousek, P.; McMaster, J.; Parker, A. W.; Towrie, M.; Sun, X.-Z.; Wilson, C.; George, M. W. *Inorg. Chem.* **2008,** *47*, 9857-9869.
10. Walsh, P. J.; Gordon, K. C.; Lundin, N. J.; Blackman, A. G. *J. Phys. Chem. A* **2005,** *109*, 5933-5942.
11. Brennaman, M. K.; Alstrum-Acevedo, J. H.; Fleming, C. N.; Jang, P.; Meyer, T. J.; Papanikolas, J. M. *J. Am. Chem. Soc.* **2002,** *124*, 15094-15098.
12. Olson, E. J. C.; Hu, D.; Hörmann, A.; Jonkman, A. M.; Arkin, M. R.; Stemp, E. D. A.; Barton, J. K.; Barbara, P. F. *J. Am. Chem. Soc.* **1997,** *119*, 11458-11467.
13. Ma, D.-L.; Che, C.-M.; Yan, S.-C. *J. Am. Chem. Soc.* **2009,** *131*, 1835-1846.
14. Brennaman, M. K.; Meyer, T. J.; Papanikolas, J. M. *J. Phys. Chem. A* **2004,** *108*, 9938-9944.
15. Song, H.; Kaiser, J. T.; Barton, J. K. *Nat Chem* **2012,** *4*, 615-620.
16. van der Salm, H.; Elliott, A. B. S.; Gordon, K. C. *Coord. Chem. Rev.* **2015,** *282–283*, 33-49.
17. Jia, C.; Liu, S. X.; Tanner, C.; Leiggener, C.; Neels, A.; Sanguinet, L.; Levillain, E.; Leutwyler, S.; Hauser, A.; Decurtins, S. *Chem. Eur. J.* **2007,** *13*, 3804-12.
18. Goze, C.; Leiggener, C.; Liu, S. X.; Sanguinet, L.; Levillain, E.; Hauser, A.; Decurtins, S. *ChemPhysChem* **2007,** *8*, 1504-12.
19. Dupont, N.; Ran, Y. F.; Jia, H. P.; Grilj, J.; Ding, J.; Liu, S. X.; Decurtins, S.; Hauser, A. *Inorg. Chem.* **2011,** *50*, 3295-303.
20. Dupont, N.; Ran, Y. F.; Liu, S. X.; Grilj, J.; Vauthey, E.; Decurtins, S.; Hauser, A. *Inorg. Chem.* **2013,** *52*, 306-12.
21. Shigehiro, T.; Yagi, S.; Maeda, T.; Nakazumi, H.; Fujiwara, H.; Sakurai, Y. *Tetrahedron Lett.* **2014,** *55*, 5195-5198.

22. Cao, K.; Lu, J.; Cui, J.; Shen, Y.; Chen, W.; Alemu, G.; Wang, Z.; Yuan, H.; Xu, J.; Wang, M.; Cheng, Y. *Journal of Materials Chemistry A* **2014,** *2*, 4945-4953.
23. Horvath, R.; Huff, G. S.; Gordon, K. C.; George, M. W. *Coord. Chem. Rev.* **2016,** *325*, 41-58.
24. Larsen, C. B.; van der Salm, H.; Clark, C. A.; Elliott, A. B. S.; Fraser, M. G.; Horvath, R.; Lucas, N. T.; Sun, X.-Z.; George, M. W.; Gordon, K. C. *Inorg. Chem.* **2014,** *53*, 1339-1354.
25. Larsen, C. B.; van der Salm, H.; Shillito, G. E.; Lucas, N. T.; Gordon, K. C. *Inorg. Chem.* **2016**.
26. Shillito, G. E.; Larsen, C. B.; McLay, J. R. W.; Lucas, N. T.; Gordon, K. C. *Inorg. Chem.* **2016,** *55*, 11170-11184.
27. Hirakawa, A. Y.; Tsuboi, M. *Science* **1975,** *188*, 359-361.
28. Clark, R. J. H.; Dines, T. J. *Angew. Chem. Int. Ed.* **1986,** *25*, 131-158.
29. van der Salm, H.; Larsen, C. B.; McLay, J. R. W.; Huff, G. S.; Gordon, K. C. *Inorg. Chim. Acta* **2015,** *428*, 1-7.
30. Dyer, J.; Blau, W. J.; Coates, C. G.; Creely, C. M.; Gavey, J. D.; George, M. W.; Grills, D. C.; Hudson, S.; Kelly, J. M.; Matousek, P.; McGarvey, J. J.; McMaster, J.; Parker, A. W.; Towrie, M.; Weinstein, J. A. *Photochem. Photobiol. Sci.* **2003,** *2*, 542.
31. Blanco-Rodríguez, A. M.; Kvapilová, H.; Sýkora, J.; Towrie, M.; Nervi, C.; Volpi, G.; Záliš, S.; Vlček, A. *J. Am. Chem. Soc.* **2014,** *136*, 5963-5973.
32. Kuimova, M. K.; Alsindi, W. Z.; Dyer, J.; Grills, D. C.; Jina, O. S.; Matousek, P.; Parker, A. W.; Portius, P.; Zhong Sun, X.; Towrie, M.; Wilson, C.; Yang, J.; George, M. W. *Dalton transactions* **2003,** 3996-4006.
33. Schoonover, J. R.; Strouse, G. F.; Dyer, R. B.; Bates, W. D.; Chen, P.; Meyer, T. J. *Inorg. Chem.* **1996,** *35*, 273-274.

The alteration of intra-ligand donor-acceptor interactions through torsional connectivity in substituted Re-dppz complexes

Supporting Information

Bethany Adams[2], Georgina E. Shillito[1], Holly van der Salm[1], Raphael Horvath[2], Christopher B. Larsen[1], Nigel T. Lucas[*1], Michael W. George[*2], Keith C. Gordon[*1].

[1]Department of Chemistry, University of Otago, P.O. Box 56, Dunedin, New Zealand. Email: keith.gordon@otago.ac.nz

[2]School of Chemistry, University of Nottingham, University Park, Nottingham, NG7 2RD, U.K. Email: mike.george@nottingham.ac.uk

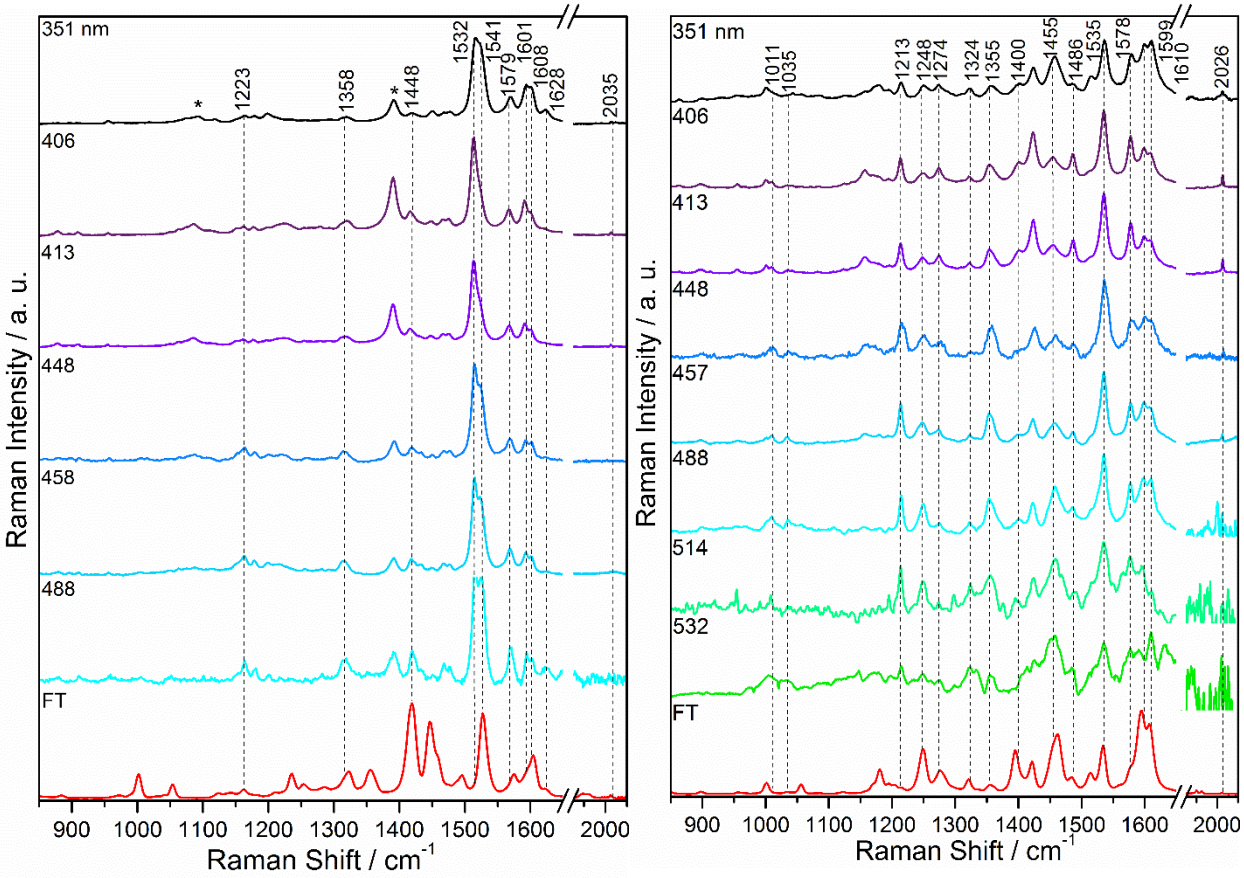

SI Figure 8. Resonance Raman spectra of $[ReCl(CO)_3(dppz\text{-}NPh_2)]$ (left) and $[ReCl(CO)_3(dppz\text{-}(TPA)_2)]$ (right), in CH_2Cl_2

PHYSICAL MEASUREMENTS

Spectroscopic grade solvents (Sigma-Aldrich) were used for all spectroscopic measurements.

Raman

Spectra were processed using GRAMS AI v8.00 (Thermo Scientific) and OriginPro v8.0 (OriginLab Corporation) software. Electronic absorption spectra were recorded in dichloromethane at room temperature, with concentration typically 1×10^{-4} M, on a Perkin Elmer Lambda950 Instrument. Raman spectroscopy FT-Raman spectra were recorded on powder samples at room temperature using a Bruker Equinox-55 interferometer with a FRA 106/5 Raman accessory. A Nd:YAG excitation source was used with 1064 nm excitation wavelength. Raman photons were detected with a D418T liquid nitrogen cooled Ge diode detector. Spectra were measured with typically 64 scans and 80 mW power, with spectral resolution of 4 cm^{-1} using the Bruker OPUS v5.5 software package. Resonance Raman spectra were recorded using a previously described setup[1-4] on CH_2Cl_2 solutions with concentrations typically 1 - 5 mM. Excitation wavelengths 350.7, 356.4, 406.7 and 413.1 nm were provided by a krypton ion laser (Innova I-302, Coherent Inc.), 457.9 nm was provided by an argon ion laser (Innova Sabre, Coherent Inc.) and 444.0 nm by a solid state diode laser (CrystaLaser).

Transient absorption and emission

Transient absorption and emission spectra were recorded on CH_2Cl_2 solutions with concentrations typically 1×10^{-5} M, which were degassed under argon for 10 minutes prior to measurement. Transients were acquired using a LP920K TA system (Edinburgh Instruments), with excitation at 355 nm from pulsed third-harmonic radiation from a Brilliant (Quantel) Nd:YAG laser at 1 Hz, and a Xe900 450 W xenon arc lamp controlled by a xP920 pulser as the probe source in TA mode. Photons were dispersed using a TMS300-A Czerny-Turner monochromator with 1800 grooves mm^{-1} grating, recorded on a R928 (Hamamatsu) photomultiplier and transcribed on a TDS3012C (Tektronix) digital oscilloscope.

Computational methods

Calculations were performed using the Gaussian09 package.[5] Geometry optimisations and harmonic vibrational frequency calculations were obtained using density functional theory (DFT), employing the CAM-B3LYP functional and a CH_2Cl_2 solvent field, using the polarisable continuum model (PCM). The LANL2DZ effective core potential and associated basis set was used for the rhenium atoms, while the 6-31G(d) basis set was used for all other atoms. Time-dependent density functional theory (TD-DFT) calculations were also performed using these parameters.

X-ray Crystallography

Single crystals of suitable for X-ray diffraction studies were obtained from diffusion of hexane into a $CHCl_3$ solution of **dppz-(TPA)$_2$**. A crystal was attached with Paratone N to a fiber loop supported in a copper mounting pin and then quenched in a cold nitrogen stream. Data were collected at 100 K using Cu K_α radiation (microsource, mirror monochromated) using an Agilent Supernova diffractometer with an Atlas detector. Data processing was undertaken with CrysAlisPro.[6] A multiscan or face-indexed absorption correction was applied to the data. The structures was solved by direct methods with SHELXS-97 and extended and refined with SHELXL-97[7-8] using the X-Seed interface.[9] The non-hydrogen atoms in the asymmetric unit were modeled with anisotropic displacement parameters, and a riding atom model with group displacement parameters was used for the hydrogen atoms. X-ray crystallographic data is available in CIF format (Supporting Information). CCDC contains the supplementary crystallographic data for this

article. These data can be obtained free of charge from The Cambridge Crystallographic Data Centre via www.ccdc.cam.ac.uk/data_request/cif.

Crystal data for **dppz-(TPA)$_2$**·2CHCl$_3$: $C_{56}H_{38}Cl_6N_6$, M = 1007.62, orange needle, 0.43 × 0.05 × 0.04 mm^3, triclinic, a = 11.6651(3) Å, b = 12.0175(3) Å, c = 18.5253(5) Å, α = 95.615(2)°, β = 101.960(2)°, γ = 109.776(2)°, V = 2350.64(9) Å^3, space group P-1 (#2), Z = 2, μ(Cu-K_α) = 3.704 mm^{-1}, $2\theta_{max}$ = 153.62°, 23927 reflections measured, 9760 independent reflections (R_{int} = 0.0338). The final $R_1(F)$ = 0.0441 (I > 2σ(I)); 0.0509 (all data). The final $wR_2(F^2)$ = 0.1182 (I > 2σ(I)); 0.1250 (all data). GoF = 1.046.

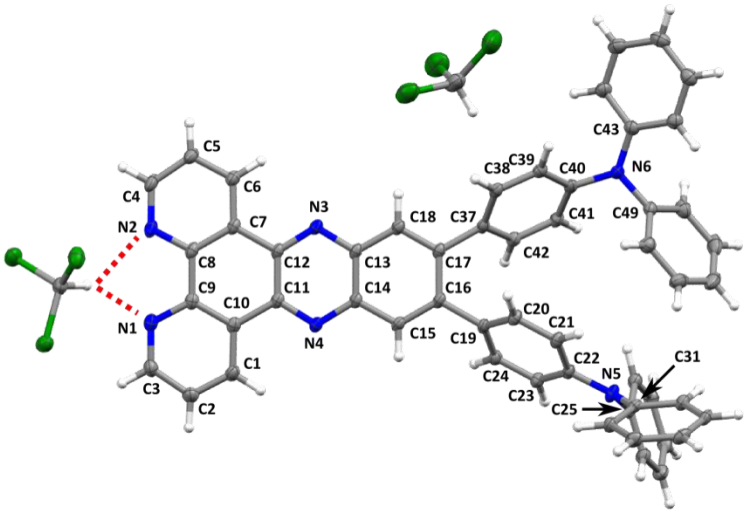

Figure S2. X-ray crystal structure of **dppz-(TPA)$_2$**. Ellipsoids are shown at 50% probability level.

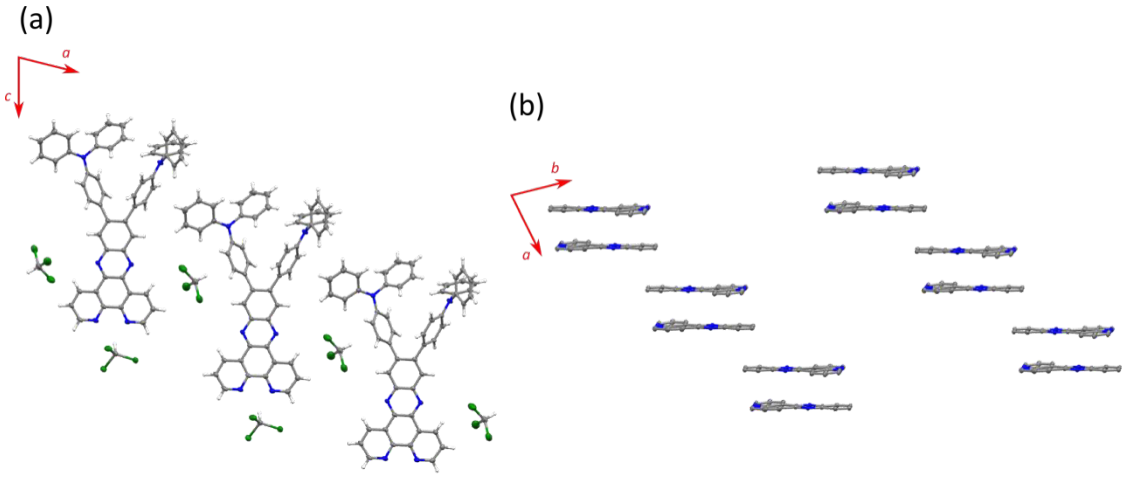

Figure S3. Crystal packing of **dppz-(TPA)$_2$**, showing (a) edge-to-edge head-to-head packing arrangement, and (b) face-to-face head-to-tail dimers. The TPA units are omitted for clarity.

Dppz-(TPA)$_2$ crystallised in the P-1 space group, co-crystallising with two molecules of $CHCl_3$ per molecule of **dppz-(TPA)$_2$** (Figure S2). The dppz skeleton is virtually planar, with a maximum deviation from planarity at C1 of 0.15 Å. The amines are essentially planar, with N5 sitting 0.08 Å above a plane defined by its *ipso* carbons (C22, C25 and C31), and N6 0.13 Å above a plane defined by its ipso carbons (C40, C43 and C49). Donor units are rotated 49.6° and 55.9° from the dppz skeleton. Terminal phenyl rings are rotated 38.9°, –124.4°, 30.3°, and –147.5° from the

bridging phenylenes. One molecule of $CHCl_3$ hydrogen-bonds with the phen-type nitrogens (2.29 Å from N1 and 2.28 Å from N2), whilst the proton of the second $CHCl_3$ interacts with the π-system of a bridging phenylene (3.14 Å from the centre of the ring defined by C37, C38, C39, C40, C41 and C42).

Crystal packing of **dppz-(TPA)$_2$** is presented in Figure S3. Two packing arrangements can be observed: (a) an edge-to-edge head-to-head packing arrangement interspersed with $CHCl_3$ clathrate, and (b) face-to-face head-to-tail dimers that exist in a "step" arrangement (3.37 Å between dppz planes in the dimers, and 3.94 Å between steps).

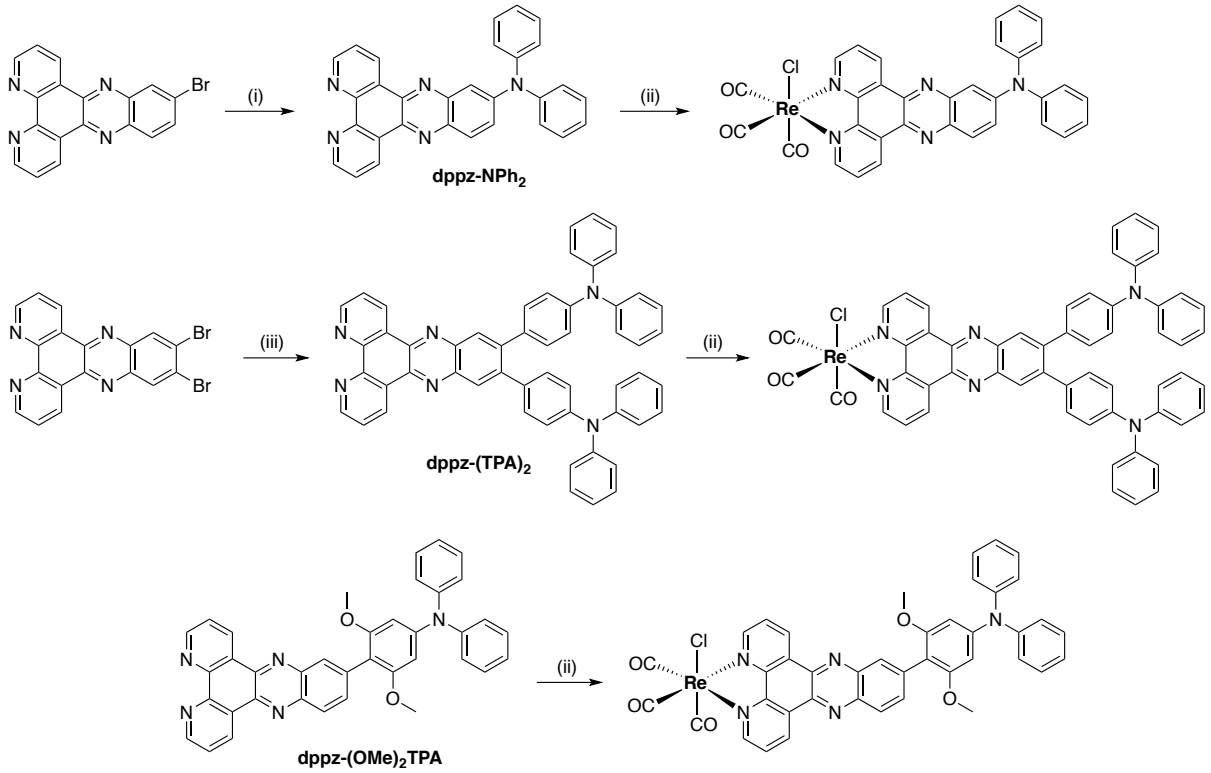

Scheme S1. Synthesis of the dppz ligands and $ReCl(CO)_3$ complexes. Reagents and conditions: (i) Diphenylamine, ^{t}BuOK, $Pd_2(dba)_3$, [^{t}Bu$_3$PH]BF_4, toluene, reflux, overnight; (ii) [$ReCl(CO)_5$], EtOH, reflux, overnight; (iii) 4-diphenylaminophenylboronic acid, K_2CO_3, $PdCl_2$(dppf), toluene, H_2O, EtOH, reflux, overnight.

General conditions and materials. 11-Bromodipyrido[3,2-*a*:2′,3′-*c*]phenazine[10], 11,12-dibromodipyrido[3,2-*a*:2′,3′-*c*]phenazine[11], 5-(4-diphenylamino-2,6-dimethoxyphenyl)benzo[*c*][1,2,5]thiadiazole[12] and 11-(4-diphenylamino-2,6-dimethoxyphenyl)dipyrido[3,2-*a*:2′,3′-*c*]phenazine (dppz-(OMe)$_2$TPA)[13] were synthesised according to literature procedures (or minor variations thereof). All other chemicals were commercially purchased and used as received unless otherwise stated. Dry solvents were obtained from a Pure-Solv MD-6 Solvent Purification system; all other solvents were AR grade. ^{1}H NMR (500 MHz) and ^{13}C NMR (126 MHz) spectra were recorded on a Varian 500 AR spectrometer at 25 °C, and are referenced to residual $CHCl_3$ (7.26 ppm) and $CDCl_3$ (77.16 ppm), respectively. ^{1}H and ^{13}C

NMR spectra were assigned using 2D spectroscopies (COSY, NOESY, ^{1}H,^{13}C-HSQC and ^{1}H,^{13}C-HMBC). ESI mass spectra were recorded on a Bruker MicrOTOF-Q mass spectrometer. Microanalyses were performed at the Campbell Microanalytical Laboratory, University of Otago, Dunedin, New Zealand.

11-Diphenylaminodipyrido[3,2-*a*:2′,3′-*c*]phenazine (dppz-NPh_2)

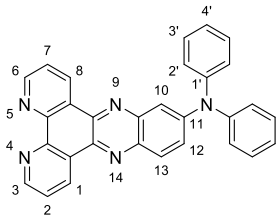

A mixture of 11-bromodipyrido[3,2-*a*:2',3'-*c*]phenazine (0.212 g, 0.59 mmol), diphenylamine (0.211 g, 1.25 mmol) and ^{t}BuOK (0.346 g, 3.08 mmol) in toluene (20 mL) was bubbled with argon for 15 min. $[^{t}Bu_3PH]BF_4$ (0.022 g, 0.076 mmol) and $Pd_2(dba)_3$ (0.031 g, 0.034 mmol) were added and the reaction mixture heated at reflux overnight under an argon atmosphere. The reaction mixture was allowed to cool to rt, the product extracted into $CHCl_3$, and washed with NH_4Cl solution (sat.), then water. The organic extract was dried over $MgSO_4$, and the solvent removed under reduced pressure. The residue was purified using preparative column chromatography (basic Al_2O_3, CH_2Cl_2) to afford dppz-NPh_2 (0.027 g, 10%) as an orange solid. The ^{1}H NMR and ESI-MS data were consistent with those previously reported.[3]

^{1}H NMR (500 MHz, $CDCl_3$): δ 9.54 (dd, *J* = 8.1, 1.8 Hz, 1H, $H_{1/8}$), 9.48 (dd, *J* = 8.1, 1.8 Hz, 1H, $H_{1/8}$), 9.21 (m, 2H, $H_{3,6}$), 8.09 (dd, *J* = 9.3, 0.4 Hz, 1H, H_{13}), 7.74 (dd, *J* = 8.1, 4.4, 1H, $H_{2/7}$), 7.70 (dd, *J* = 8.1, 4.5, 1H, $H_{2/7}$), 7.68 (dd, *J* = 9.2, 2.6 Hz, 1H, H_{12}), 7.64 (dd, *J* = 2.6, 0.4 Hz, 1H, H_{10}), 7.40 (dd, *J* = 8.5, 7.5 Hz, 4H, $H_{3'}$), 7.29 (dd, *J* = 8.5, 1.1 Hz, 4H, $H_{2'}$), 7.22 (tt, *J* = 7.4, 1.2 Hz, 2H, $H_{4'}$) ppm. HRMS (ESI) calcd for $C_{30}H_{19}N_5Na$ ($[M+Na]^+$): m/z 472.153. Found: m/z 472.152.

fac-Chlorotricarbonyl(11-diphenylaminodipyrido-[3,2-*a*:2′,3′-*c*]phenazine)rhenium(I) ([$ReCl(CO)_3$(dppz-NPh_2)])

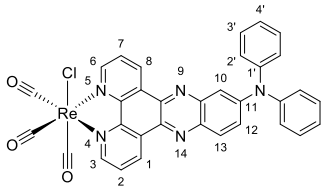

A mixture of dppz-NPh_2 (0.101g, 0.225 mmol) and [$ReCl(CO)_5$] (0.081 g, 0.225 mmol) in EtOH (100 mL) was heated at reflux overnight. The reaction was allowed to cool to rt, and the resultant precipitate filtered and washed with EtOH to afford [$ReCl(CO)_3$(dppz-NPh_2)] (0.154 g, 91%) as a purple solid.

^{1}H NMR (500 MHz, $CDCl_3$): *δ* 9.70 (m, 2H, $H_{1,8}$), 9.39 (m, 2H, $H_{3,6}$), 8.13 (d, *J* = 9.4 Hz, 1H, H_{13}), 7.93 (m, 2H, $H_{2,7}$), 7.78 (dd, *J* = 9.4, 2.6 Hz, 1H, H_{12}), 7.59 (d, *J* = 2.6 Hz, 1H, H_{10}), 7.45 (dd, *J* = 8.3, 7.5 Hz, 4H, $H_{3'}$), 7.33 (dd, *J* = 8.4, 1.0 Hz, 4H, $H_{2'}$), 7.29 (tt, *J* = 7.4, 1.1 Hz, 2H, $H_{4'}$) ppm. ^{13}C NMR (126 MHz, $CDCl_3$): *δ* 197.07 (CO_{eq}), 189.56 (CO_{ax}), 154.05 ($C_{3/6}$), 153.42 ($C_{3/6}$), 151.38 (C_{11}), 149.30 ($C_{4a/4b}$), 148.41 ($C_{4a/4b}$), 145.98 ($C_{1'}$), 145.05 (C_{9a}), 140.17 (C_{13a}), 139.55 ($C_{8b/14a}$), 136.41 ($C_{8b/14a}$), 135.79 ($C_{1/8}$), 135.17 ($C_{1/8}$), 131.05 ($C_{8a/14b}$), 130.67 ($C_{8a/14b}$), 130.21 ($C_{3'}$), 130.17 (C_{13}), 128.62 (C_{12}), 126.81 ($C_{2/7}$), 126.63 ($C_{2/7}$), 126.61 ($C_{2'}$), 126.03 ($C_{4'}$), 113.37 (C_{10}) ppm. HRMS (ESI) calcd for $C_{33}H_{19}ClN_5NaO_3Re$

([M+Na]$^+$): m/z 778.062. Found: 778.066. Elemental analysis calcd for $C_{33}H_{19}ClN_5O_3Re{\cdot}0.5H_2O$: C, 51.86; H, 2.64; N, 9.16. Found: C, 51.93; H, 2.60; N, 9.02.

11,12-Di(4-diphenylaminophenyl)dipyrido[3,2-*a*:2′,3′-*c*]phenazine (dppz-(TPA)$_2$)

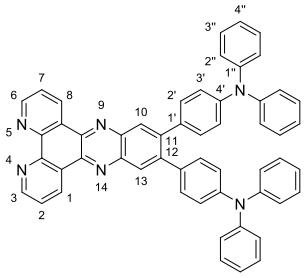

A mixture of 11,12-dibromodipyrido[3,2-*a*:2′,3′-*c*]phenazine (0.417 g, 0.947 mmol), 4-diphenylaminophenylboronic acid (1.17 g, 4.04 mmol) and K_2CO_3 (1.30 g, 9.41 mmol) in toluene (20 mL), H_2O (10 mL) and EtOH (5 mL) was bubbled with argon for 15 min. $PdCl_2$(dppf) (0.160 g, 0.195 mmol) was added and the reaction mixture heated at reflux overnight under an argon atmosphere. The reaction mixture was allowed to cool, and the product extracted into $CHCl_3$, and washed with NH_4Cl solution (sat.), then water. The organic extract was dried over $MgSO_4$, and the solvent removed under reduced pressure. The residue was purified using preparative column chromatography (basic Al_2O_3, 5% MeOH in $CHCl_3$) to afford dppz-(TPA)$_2$ (0.568 g, 78%) as an orange solid.

^{1}H NMR (500 MHz, $CDCl_3$): δ 9.61 (d, J = 7.9 Hz, 2H, $H_{1,8}$), 9.27 (m, 2H, $H_{3,6}$), 8.34 (s, 2H, $H_{10,13}$), 7.79 (dd, J = 7.8, 4.1 Hz, 2H $H_{2,7}$), 7.28 (t, J = 7.7 Hz, 8H, $H_{3''}$), 7.21 (d, J = 8.2 Hz, 4H, $H_{2'}$), 7.15 (d, J = 8.3 Hz, 8H, $H_{2''}$), 7.06 (t, J = 7.2 Hz, 4H, $H_{4''}$), 7.05 (d, J = 8.1 Hz, 4H, $H_{3'}$) ppm. ^{13}C NMR (126 MHz, $CDCl_3$): δ 152.36 ($C_{3,6}$), 147.93 ($C_{4a,4b}$), 147.64 ($C_{1''}$), 147.46 ($C_{4'}$), 144.54 ($C_{11,12}$), 142.05 ($C_{9a,13a}$), 141.13 ($C_{8b,14a}$), 134.06 ($C_{1,8}$), 134.03 ($C_{1'}$), 130.94 ($C_{2'}$), 129.80 ($C_{10,13}$), 129.51 ($C_{3''}$), 127.92 ($C_{8a,14b}$), 124.83 ($C_{2''}$), 124.37 ($C_{2,7}$), 123.37 ($C_{4''}$), 122.69 ($C_{3'}$) ppm. HRMS (ESI) calcd for $C_{54}H_{37}N_6$ ([M+H]$^+$): m/z 769.307. Found: m/z 769.311. Elemental analysis calcd for $C_{54}H_{36}N_6{\cdot}CHCl_3$: C, 74.37; H, 4.20; N, 9.46. Found: C, 74.12; H, 4.57; N, 9.11.

fac-Chlorotricarbonyl(11,12-di(4-diphenylaminophenyl)dipyrido[3,2-*a*:2′,3′-*c*]phenazine)rhenium(I) ([ReCl(CO)$_3$(dppz-(TPA)$_2$)])

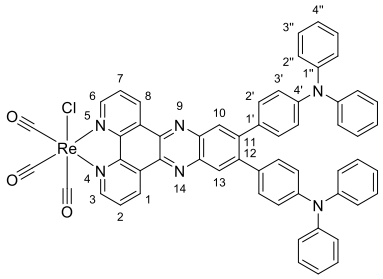

A mixture of dppz-(TPA)$_2$ (0.118 g, 0.153 mmol) and [ReCl(CO)$_5$] (0.065 g, 0.180 mmol) in EtOH (200 mL) was heated at reflux overnight. The reaction mixture was allowed to cool, and the precipitate filtered and washed with EtOH to afford [ReCl(CO)$_3$(dppz(TPA)$_2$)] (0.104 g, 63%) as a purple solid.

^{1}H NMR (500 MHz, $CDCl_3$): δ 9.82 (dd, J = 8.2, 1.4 Hz, 2H, $H_{1,8}$), 9.45 (dd, J = 5.2, 1.4 Hz, 2H, $H_{3,6}$), 8.42 (s, 2H, $H_{10,13}$), 8.01 (dd, J = 8.2, 5.2 Hz, 2H, $H_{2,7}$), 7.30 (t, J = 7.4 Hz, 8H, $H_{3''}$), 7.21 (d, J = 8.7 Hz, 4H, $H_{2'}$), 7.15 (dd, J = 8.5, 1.0 Hz, 8H, $H_{2''}$), 7.08 (tt, J = 7.3, 1.2 Hz, 4H, $H_{4''}$), 7.06 (d, J = 8.6 Hz, 4H, $H_{3'}$) ppm. ^{13}C NMR (126 MHz, $CDCl_3$): δ 197.00 (CO_{eq}), 189.46 (CO_{ax}), 154.22 ($C_{3,6}$), 149.32 ($C_{4a,4b}$), 147.88 ($C_{4'}$), 147.51 ($C_{1''}$), 146.29 ($C_{11,12}$), 142.59 ($C_{9a,13a}$), 139.23 ($C_{8b,14a}$), 135.79 ($C_{1,8}$), 133.31 ($C_{1'}$), 130.88 ($C_{2'}$), 130.84 ($C_{8a,14b}$), 129.87 ($C_{10,13}$), 129.57 ($C_{3''}$), 126.98 ($C_{2,7}$), 125.02 ($C_{2''}$), 123.60 ($C_{4''}$), 122.43 ($C_{3'}$) ppm. HRMS (ESI) calcd for $C_{57}H_{38}N_6O_4Re$ ([M-Cl+H_2O]$^+$): *m/z* 1057.251. Found: *m/z* 1057.256. Elemental analysis calcd for $C_{57}H_{36}ClN_6O_3Re$: C, 63.71; H, 3.38; N, 7.82. Found: C, 63.68; H, 3.40; N, 7.69.

fac-Chlorotricarbonyl(11-(4-Diphenylamino-2,6-dimethoxyphenyl)dipyrido[3,2-*a*:2′,3′-*c*]phenazine)rhenium(I) ([ReCl(CO)$_3$(dppz-(OMe)$_2$TPA)])

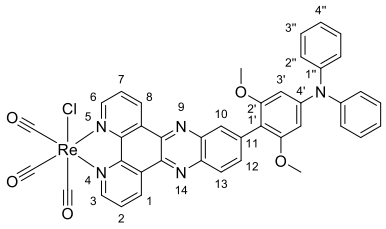

A mixture of dppz-(OMe)$_2$TPA (0.056 g, 0.155 mmol) and [ReCl(CO)$_5$] (0.082 g, 0.140 mmol) in EtOH (100 mL) was heated at reflux overnight. The reaction mixture was allowed to cool, and the precipitate filtered and washed with EtOH to afford [ReCl(CO)$_3$(dppz-(OMe)$_2$TPA)] (0.058 g, 42%) as an orange solid.

^{1}H NMR (500 MHz, $CDCl_3$): δ 9.86 (m, 2H, $H_{1,8}$), 9.44 (m, 2H, $H_{3,6}$), 8.46 (d, J = 1.8 Hz, 1H, H_{10}), 8.37 (d, J = 8.9 Hz, 1H, H_{13}), 8.12 (dd, J = 8.9, 1.8 Hz, 1H, H_{12}), 8.00 (m, 2H, $H_{2,7}$), 7.34 (t, 7.0 Hz, 4H, $H_{3''}$), 7.24 (d, J = 7.8 Hz, 4H, $H_{2''}$), 7.11 (t, J = 7.2 Hz, 2H, $H_{4''}$), 6.42 (s, 2H, $H_{3'}$), 3.64 (s, 6H, O*Me*) ppm. ^{13}C NMR (126 MHz, $CDCl_3$): δ 197.04 (CO_{eq}), 189.50 (CO_{ax}), 158.20 ($C_{2'}$), 154.14 ($C_{3/6}$), 154.06 ($C_{3/6}$), 150.17 ($C_{4'}$), 149.33 ($C_{4a/4b}$), 149.21 ($C_{4a/4b}$), 147.39 ($C_{1''}$), 143.23 (C_{9a}), 142.40 (C_{13a}), 139.45 (C_{11}), 138.94 ($C_{8b/14a}$), 138.57 ($C_{8b/14a}$), 137.36 (C_{12}), 135.93 ($C_{1/8}$), 135.81 ($C_{1/8}$), 131.47 (C_{10}), 130.99 ($C_{8a/14b}$), 130.95 ($C_{8a/14b}$), 129.54 ($C_{3''}$), 128.13 (C_{13}), 126.93 ($C_{2/7}$), 126.87 ($C_{2/7}$), 125.32 ($C_{2''}$), 123.83 ($C_{4''}$), 111.45 ($C_{1'}$), 99.47 ($C_{3'}$), 56.07 (O*Me*) ppm. HRMS (ESI) calcd for $C_{41}H_{29}N_5O_6Re$ ([M-Cl+H_2O]$^+$): *m/z* 874.167. Found: *m/z* 874.172. Elemental analysis calcd for $C_{41}H_{27}ClN_5O_5Re{\cdot}0.5H_2O$: C, 54.69; H, 3.13; N, 7.78. Found: C, 54.33; H, 3.41; N, 7.83.

1. Howell, S. L.; Gordon, K. C. *J. Phys. Chem. A* **2004,** *108*, 2536-2544.
2. Lind, S. J.; Gordon, K. C.; Waterland, M. R. *J. Raman Spectrosc.* **2008,** *39*, 1556-1567.
3. Lind, S. J.; Walsh, T. J.; Blackman, A. G.; Polson, M. I. J.; Irwin, G. I. S.; Gordon, K. C. *J. Phys. Chem. A* **2009,** *113*, 3566-3575.
4. Horvath, R.; Gordon, K. C. *Coord. Chem. Rev.* **2010,** *254*, 2505-2518.
5. Frisch, M. J.; Trucks, G. W.; Schlegel, H. B.; Scuseria, G. E.; Robb, M. A.; Cheeseman, J. R.; Scalmani, G.; Barone, V.; Mennucci, B.; Petersson, G. A.; Nakatsuji, H.; Caricato, M.; Li, X.; Hratchian, H. P.; Izmaylov, A. F.; Bloino, J.; Zheng, G.; Sonnenberg, J. L.; Hada, M.; Ehara, M.; Toyota, K.; Fukuda, R.; Hasegawa, J.; Ishida, M.; Nakajima, T.; Honda, Y.; Kitao, O.; Nakai, H.; Vreven, T.; Montgomery Jr., J. A.; Peralta, J. E.; Ogliaro, F.; Bearpark, M. J.; Heyd, J.; Brothers, E. N.; Kudin, K. N.; Staroverov, V. N.; Kobayashi, R.; Normand, J.; Raghavachari, K.; Rendell, A. P.; Burant, J. C.; Iyengar, S. S.; Tomasi, J.; Cossi, M.; Rega, N.; Millam, N. J.; Klene, M.; Knox, J. E.; Cross, J. B.; Bakken, V.; Adamo, C.; Jaramillo, J.; Gomperts, R.; Stratmann, R. E.; Yazyev, O.; Austin, A. J.; Cammi, R.; Pomelli, C.; Ochterski, J. W.; Martin, R. L.; Morokuma, K.; Zakrzewski, V. G.; Voth, G. A.; Salvador, P.; Dannenberg, J. J.; Dapprich, S.; Daniels, A. D.; Farkas, Ö.; Foresman, J. B.; Ortiz, J. V.; Cioslowski, J.; Fox, D. J. *Gaussian 09*, Gaussian, Inc.: Wallingford, CT, USA, 2009.
6. *CrysAlisPro*, version 1.171.36.28; Agilent Technologies: Yarnton, Oxfordshire, UK, 2013.
7. Sheldrick, G. M. *SHELX-97 Programs for Crystal Structure Analysis*, Göttingen, Germany, 1998.
8. Sheldrick, G. M. *Acta Crystallogr A* **2008,** *64*, 112-122.
9. Barbour, L. J. *Journal of Supramolecular Chemistry* **2001,** *1*, 189-191.
10. Walsh, P. J.; Gordon, K. C.; Lundin, N. J.; Blackman, A. G. *J. Phys. Chem. A* **2005,** *109*, 5933-5942.
11. Schafer, B.; Gorls, H.; Presselt, M.; Schmitt, M.; Popp, J.; Henry, W.; Vos, J. G.; Rau, S. *Dalton transactions* **2006,** 2225-2231.
12. Barnsley, J. E.; Shillito, G. E.; Larsen, C. B.; van der Salm, H.; Wang, L. E.; Lucas, N. T.; Gordon, K. C. *J. Phys. Chem. A* **2016,** *120*, 1853-66.
13. Shillito, G. E.; Larsen, C. B.; McLay, J. R. W.; Lucas, N. T.; Gordon, K. C. *Inorg. Chem.* **2016,** *55*, 11170-11184.